Linking Atmospheric Cloud Radiative Effects, Tropical Precipitation, and Column Relative Humidity

Michael Robert Needham[1,1] and David Allan Randall[1,1]

[1]Colorado State University

November 30, 2022

Abstract

Work in recent decades has demonstrated a robust relationship between tropical precipitation and the column relative humidity (CRH). This study identifies a similar relationship between CRH and the atmospheric cloud radiative effect (ACRE) calculated from satellite observations. Like precipitation, the ACRE begins to increase rapidly when CRH exceeds a critical value near 75\%. We show that the ACRE can be estimated from CRH, similar to the way that CRH has been used to estimate precipitation. Our method reproduces the annual mean spatial structure of ACRE in the tropics, and skillfully estimates the mean ACRE on monthly and daily time scales in six regions of the tropics. We propose that the exponential dependence of precipitation on CRH is a result of cloud-longwave feedbacks, which facilitate a shift from convective to stratiform conditions.

Linking Atmospheric Cloud Radiative Effects and Tropical Precipitation

Michael R. Needham[1], **David A. Randall**[1]

[1]Department of Atmospheric Science, Colorado State University, Fort Collins, CO, USA

Key Points:

- The atmospheric cloud radiative effect (ACRE) depends on the column relative humidity (CRH) in a way similar to precipitation
- The CRH skillfully estimates ACRE on annual, monthly, and daily time scales in the tropics
- ACRE-cloud feedback suggested to explain the CRH-precipitation relationship by facilitating a shift from convective to stratiform rainfall

Corresponding author: Michael R. Needham, `m.needham@colostate.edu`

Abstract

Work in recent decades has demonstrated a robust relationship between tropical precipitation and the column relative humidity (CRH). This study identifies a similar relationship between CRH and the atmospheric cloud radiative effect (ACRE) calculated from satellite observations. Like precipitation, the ACRE begins to increase rapidly when CRH exceeds a critical value near 75%. We show that the ACRE can be estimated from CRH, similar to the way that CRH has been used to estimate precipitation. Our method reproduces the annual mean spatial structure of ACRE in the tropics, and skillfully estimates the mean ACRE on monthly and daily time scales in six regions of the tropics. We propose that the exponential dependence of precipitation on CRH is a result of cloud-longwave feedbacks, which facilitate a shift from convective to stratiform conditions.

Plain Language Summary

The tropical precipitation rate can be estimated using a quantity called the column relative humidity (CRH), which quantifies how close the atmosphere is to becoming saturated with water. We show that the CRH can also be used to estimate the local radiative heating of the atmosphere due to clouds. Our simple method can reproduce the average cloud radiative heating of the tropical atmosphere, and we use it to estimate the monthly average and daily average heating in six different tropical regions. We suggest that the relationship between precipitation and CRH is caused by cloud-radiative heating, which promotes precipitation in large-scale systems.

1 Introduction

The effects of clouds on the Earth's radiation balance can be quantified using the cloud radiative effect (CRE), defined as the difference between full-sky and clear-sky radiative fluxes (Ramanathan, 1987). The CRE manifests at the top of the atmosphere, where clouds increase the reflection of solar radiation while they simultaneously enhance greenhouse warming; at the surface, where cloud shading prevents solar absorption at the ground at the same time as clouds emit infrared radiation downwards; or in the atmosphere itself, where clouds warm or cool locally by absorbing or emitting radiation. A large body of work has investigated the impact of this atmospheric cloud radiative effect (ACRE) on the Earth's global circulation patterns (Slingo & Slingo, 1988; Randall

et al., 1989; Sherwood et al., 1994; Stevens et al., 2012; Li et al., 2015; Voigt & Albern, 2019). For example, the ACRE has been found to widen the subsiding branches of the Hadley cells and to narrow the Intertropical Convergence Zone (ITCZ) in idealized numerical simulations (Harrop & Hartmann, 2016; Popp & Silvers, 2017; Albern et al., 2018; Dixit et al., 2018).

The longwave ACRE has been identified as an important feedback mechanism in the context of the persistence of convective self-aggregation, the initial development of tropical cyclones, and the Madden–Julian Oscillation (Bretherton et al., 2005; Chikira, 2014; Arnold & Randall, 2015; Wolding et al., 2016; Wing et al., 2017; Khairoutdinov & Emanuel, 2018; Emanuel, 2019; Ruppert et al., 2020; Benedict et al., 2020; Medeiros et al., 2021). The longwave ACRE can be a strong localized atmospheric heating which induces a thermally direct circulation connecting humid and dry regions. This circulation transports moisture against the gradient into humid regions, which allows for increased precipitation and cloudiness.

Observational and modeling studies in recent decades have shown a strong link between atmospheric humidity and tropical precipitation (Zeng, 1999; Raymond, 2000; Bretherton et al., 2004; Raymond & Zeng, 2005; Raymond et al., 2009; Ahmed & Schumacher, 2015; Rushley et al., 2018; Powell, 2019; Wolding et al., 2020). Bretherton et al. (2004) demonstrated that the mean precipitation rate derived from satellite observations was a strong function of the column relative humidity (CRH, defined as the ratio between the water vapor path and saturation water vapor path). They showed that tropical precipitation could be modeled as an exponential function of CRH, and this relationship has been used in many applications including theoretical studies of the MJO (see Rushley et al. (2018), and references therein). More recently, Ahmed and Schumacher (2015) used observations from the DYNAMO field campaign (Yoneyama et al., 2013) and satellite estimates of precipitation to show that the rapid increase of precipitation in humid regions is due to stratiform rather than convective rainfall. Furthermore, they found that the area covered by stratiform precipitation accounted for much of the non-linearity in the precipitation-humidity relationship, while the area covered by convective precipitation was only weakly non-linear with CRH.

Our goal in this study is to suggest a link between longwave-cloud feedbacks and the observed relationship between tropical precipitation and CRH, which will be further

examined in a companion paper. Section 2 provides a description of data. In section 3, the ACRE is shown to be a strong function of the CRH, which suggests that the CRH can be used to estimate the ACRE. This possibility is explored in section 4, where the estimate is evaluated on annual mean, monthly, and daily time scales. We also suggest that the exponential relationship between CRH and tropical precipitation is a necessary consequence of the longwave cloud feedback described in previous studies which facilitate a shift from convective to stratiform precipitation. Conclusions are discussed in section 5.

2 Data and Methods

The analysis in this study utilizes two primary data sources. Top of atmosphere and surface fluxes of longwave and shortwave radiation come from the CERES SYN1deg Ed4a product (Doelling et al. (2013), hereafter CERES). CERES data were downloaded on a 1°×1° grid at a daily mean temporal resolution. Radiative fluxes were used to calculate the CRE as the difference between full-sky and clear-sky fluxes. The CRE was evaluated at the top of atmosphere and at the surface, and the ACRE was calculated as the difference between the two.

Reanalysis fields of temperature and specific humidity were downloaded from ERA5 (Hersbach et al., 2018, 2020) at a temporal resolution of 6 hours on the native 0.25°×0.25° grid. The CRH was calculated as

$$\mathrm{CRH} = \frac{\int_{p_t}^{p_s} q dp}{\int_{p_t}^{p_s} q^*(T) dp}, \tag{1}$$

where q^* is the saturation vapor pressure. The ERA5 data were averaged to daily means and to the coarser 1°×1° CERES grid.

Both data sources span the same 19-year period from January 1, 2001 through December 31, 2019. Analysis was restricted to the tropical belt ranging from 30°S to 30°N. In addition to the tropical belt, the analysis was repeated for six subset regions which represent the Indo-Pacific warm pool, the Pacific ITCZ, the south Pacific convergence zone (hereafter SPCZ), the Pacific cold tongue, the Atlantic ITCZ, and the Atlantic cold tongue.

In addition to these two sources, precipitation rates from the TRMM Multisatellite Precipitation Analysis 3B42 product (Huffman et al. (2016) hereafter TRMM) were used to show a climatology and to visualize the exponential pickup of precipitation with CRH described in the introduction. The TRMM data cover the same 19-year period and were averaged to align with the 1°×1° CERES grid.

3 ACRE binned by CRH

The tropical band ranging from 30°S to 30°N contains regions with distinct distributions of precipitation and humidity (Figs. 1.a and 1.b) These include regions of warm SSTs with enhanced convection (such as the Indo-Pacific warm pool, the SPCZ, and the Atlantic and Pacific portions of the ITCZ), and regions of cool SSTs with suppressed convection (such as the Atlantic and Pacific cold tongues). Land surface covers approximately 25% of this belt which introduces additional complexity due to factors such as a stronger diurnal cycle and monsoons.

To see how precipitation and ACRE vary with CRH over the tropical belt we perform a binning analysis, following the method used in previous studies. The area-weighted average TRMM precipitation rate was found for each CRH bin of width 2% ranging from 0% to 100%. The 25^{th} and 75^{th} percentiles were also found as a measure of the spread of precipitation in each bin. This procedure was repeated for the net, longwave, and shortwave ACRE over the entire tropical belt with results shown in Figs 1.c through 1.f.

The net ACRE (Fig. 1.d) is negative or zero when the CRH is small, due to longwave and shortwave contributions which mostly offset (Figs 1.e and 1.f). When the CRH becomes large the longwave component changes sign and begins to increase. The shortwave component increases as well, but at a slower rate. The combination of the two terms leads to a rapid increase of the net ACRE above a threshold of about 60% CRH. The rapid pickup in ACRE is evocative of the dependence of precipitation on CRH (Fig. 1.c). As will be discussed in section 4.3, this similarity is not a coincidence, but is likely the result of a longwave-cloud feedback in humid regions of the tropics that promotes a shift from convective to stratiform precipitation. While the precipitation appears to depend exponentially on the CRH, dependence of the ACRE more closely resembles a linear relationship above the threshold level.

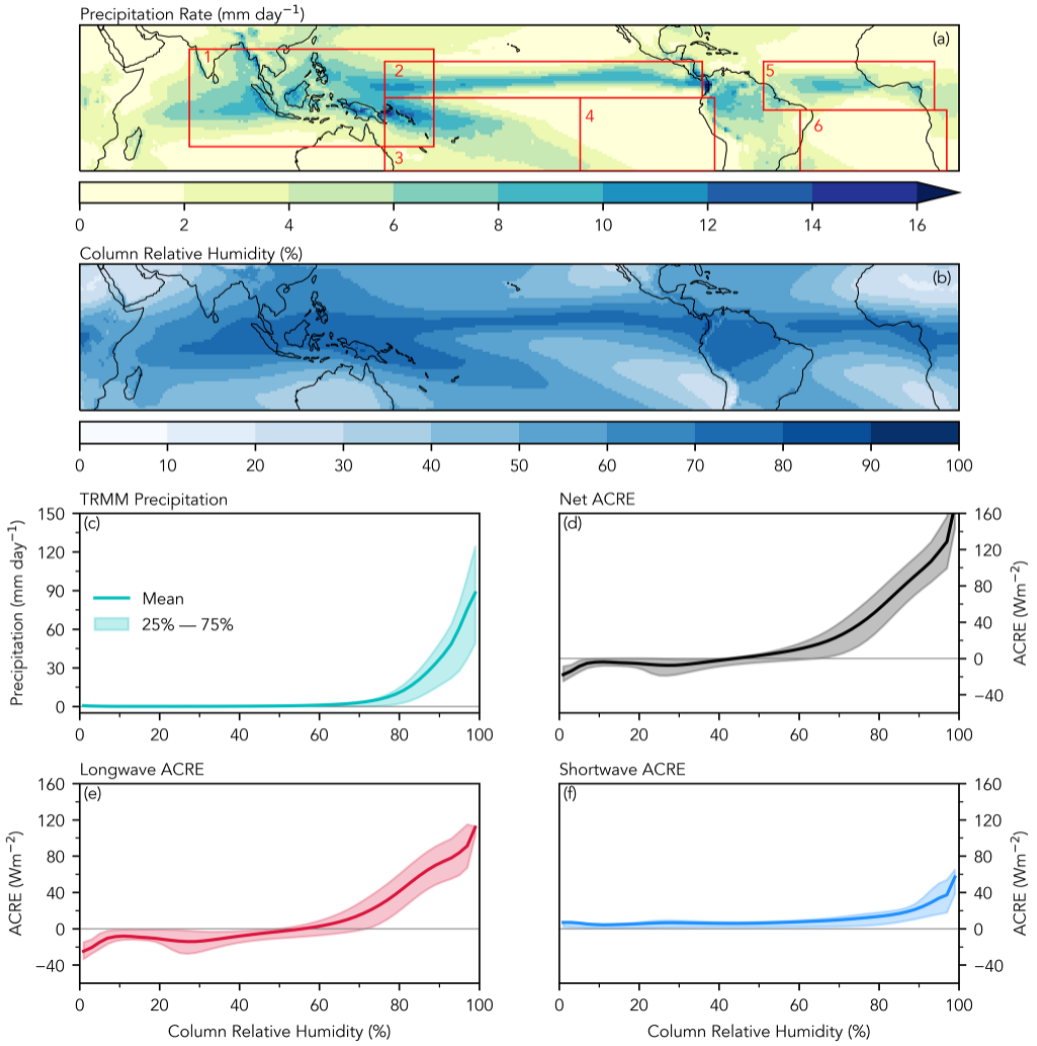

Figure 1. **(a):** Annual mean precipitation rate from 2001 through 2019, calculated using the TRMM 3b42 product (Huffman et al., 2016). Boxes 1 - 6 show the boundaries of six regions used in section 4.2, with specific boundaries recorded in Tbl. S1. **(b):** Annual mean column relative humidity calculated from ERA5 reanalysis. **(c):** TRMM Precipitation rate binned by CRH for the belt ranging from 30°S to 30°N. The shaded area shows the region bounded by the 25th and 75th percentiles for each CRH bin. **(d):** Same as **(c)**, but for the ACRE. **(e)** and **(f):** ACRE from **(d)**, decomposed into longwave and shortwave components.

A comparison of Figs. 1.e and 1.f shows that the ACRE is largely determined by the absorption of longwave radiation, consistent with previous studies (Slingo & Slingo, 1988; Allan, 2011). When this analysis is repeated for the six regions shown in Fig. 1.a, nearly identical curves are returned, even though the regions have markedly different distributions of CRH (Fig. S1 and S2 of supporting information). The only obvious difference in the regional curves is due to the influence of marine stratus clouds in the cold tongue regions (Klein & Hartmann, 1993), which have a large shortwave ACRE and tend to be found in regions with low CRH.

4 Estimating ACRE from CRH

The 25^{th} and 75^{th} percentiles of the ACRE in Fig. 1.d are close to the mean value, which suggests little spread in the distribution of ACRE at a particular CRH. This indicates that the CRH may be used to estimate the ACRE, similar to how it has been used to estimate tropical precipitation. To estimate the ACRE, the daily mean CRH at a grid cell at a particular timestep was mapped onto the curves in Figs. 1.e and 1.f to give an estimate of the longwave and shortwave components. These two fields were then added together to give the daily mean net ACRE at each grid cell.

It is possible that a different method which uses an optimized rectifier or exponential fit may give a better estimation of the ACRE. Additionally, a method that takes into account the total condensed liquid or ice water path to help separate low and high clouds may more accurately estimate the ACRE and help to remove regional biases. These possibilities are left for future work because our purpose here is only to demonstrate that the CRH can plausibly estimate the ACRE.

4.1 Time Mean Estimation of ACRE

Fig. 2.a shows the annual mean ACRE calculated from the observed CERES fluxes. The ACRE is positive over the Indo-Pacific, SPCZ and ITCZ regions due to the absorption of longwave radiation by convective clouds and organized systems. In the cold-tongue regions the reflection of sunlight by marine stratus clouds reduces the shortwave radiation that would otherwise been absorbed, which leads to a negative ACRE. The cooling albedo effect is smaller than the warming greenhouse effect so that the ACRE averaged over the 30°S to 30°N belt is 15.193 W m^{-2}. In Fig. 2.b the time mean of the

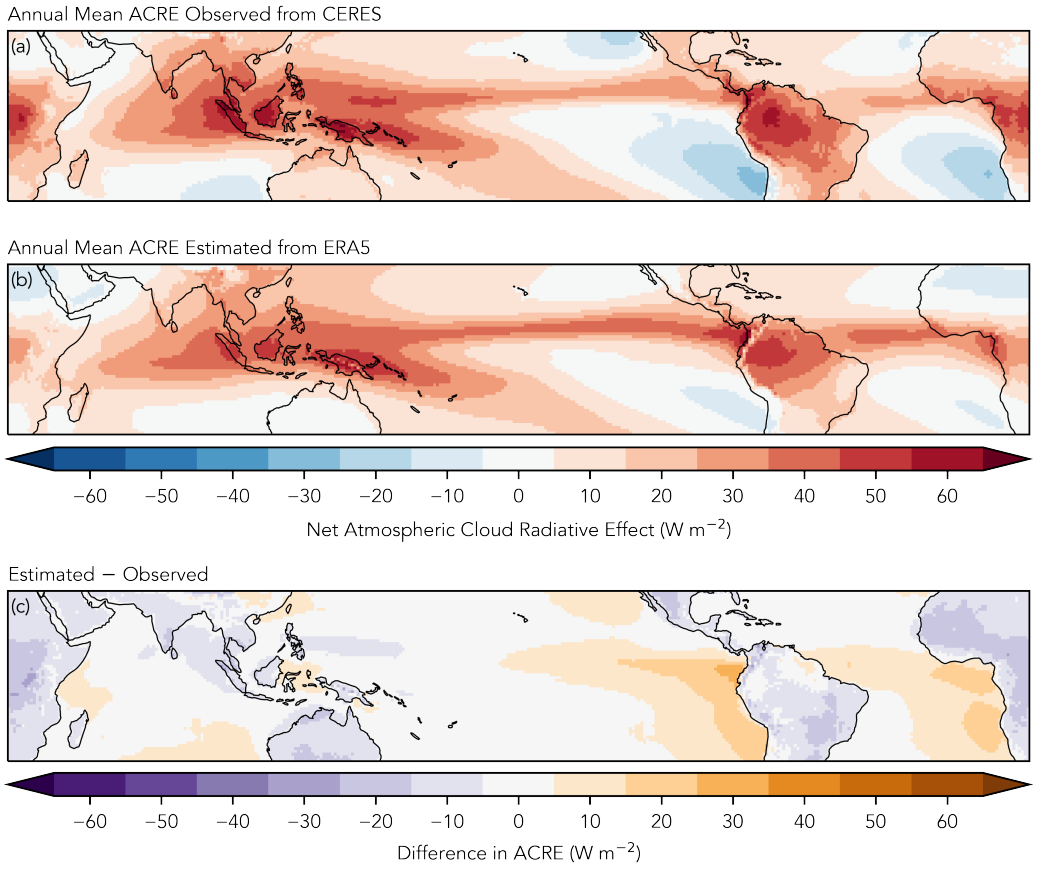

Figure 2. **(a):** Annual mean ACRE calculated from CERES radiative fluxes. **(b):** Same as **(a)**, but estimated from ERA5 column relative humidity. **(c):** Difference calculated as panel **(b)** minus panel **(a)**.

estimated ACRE is shown. The estimated ACRE largely reproduces the same spatial structure as the observed ACRE, which includes large positive values over the Indo-Pacific, SPCZ, and ITCZ regions, and negative values in the marine stratus regions. The annual mean ACRE estimated from CRH is 15.203 W m^{-2}, which is an error of only about 0.01 W m^{-2} compared to the ACRE calculated from satellite observations.

The difference between the estimated and observed ACRE is shown in Fig. 2.c, which shows that the small error in the domain averaged ACRE is due to positive and negative errors that largely cancel. The estimation method appears to have a positive bias in the east Pacific relative to the west Pacific. This is partially due to the longwave CRE at the top of the atmosphere (not shown), and is consistent with Kubar et al. (2007) who found that the temperature of high tropical clouds in the east Pacific was about 5 K warmer compared to similar clouds in the west Pacific. In addition, the estimation method gives negative errors over land compared to mostly positive errors over oceans. Although the errors discussed here are not negligible, we emphasize that this is merely the first attempt to estimate the ACRE from the CRH.

4.2 Accuracy of the Estimation on Shorter Time Scales

The estimation largely reproduces the annual mean spatial structure of the ACRE. How well does it perform on shorter time scales? To answer this, Fig. 3 compares the observed and estimated monthly mean ACRE anomaly for each of the six regions outlined in Fig. 1.a. Anomalies were calculated as the monthly average ACRE over the region minus the annual mean ACRE for that region for each month, which effectively removes the seasonal cycle. The agreement between the observed and estimated ACRE was evaluated using Pearson's R^2 correlation, which is shown in the lower left-hand corner of each panel.

The Indo-Pacific, SPCZ, and both ITCZ regions each show a high degree of correlation, with R^2 greater than either 0.6 or 0.7. The estimation method is able to account for the large peaks in magnitude in the warm pool and pacific ITCZ regions in 2010 and 2015 to 2016 which are likely associated with the strong El Niño events of those years (National Weather Service (2020), see Figs. S3 through S6 from supporting information). The correlation is slightly lower for the cold tongue regions, with R^2 equal to 0.56 and 0.515 in the Pacific and Atlantic, respectively. Together, this indicates that more than

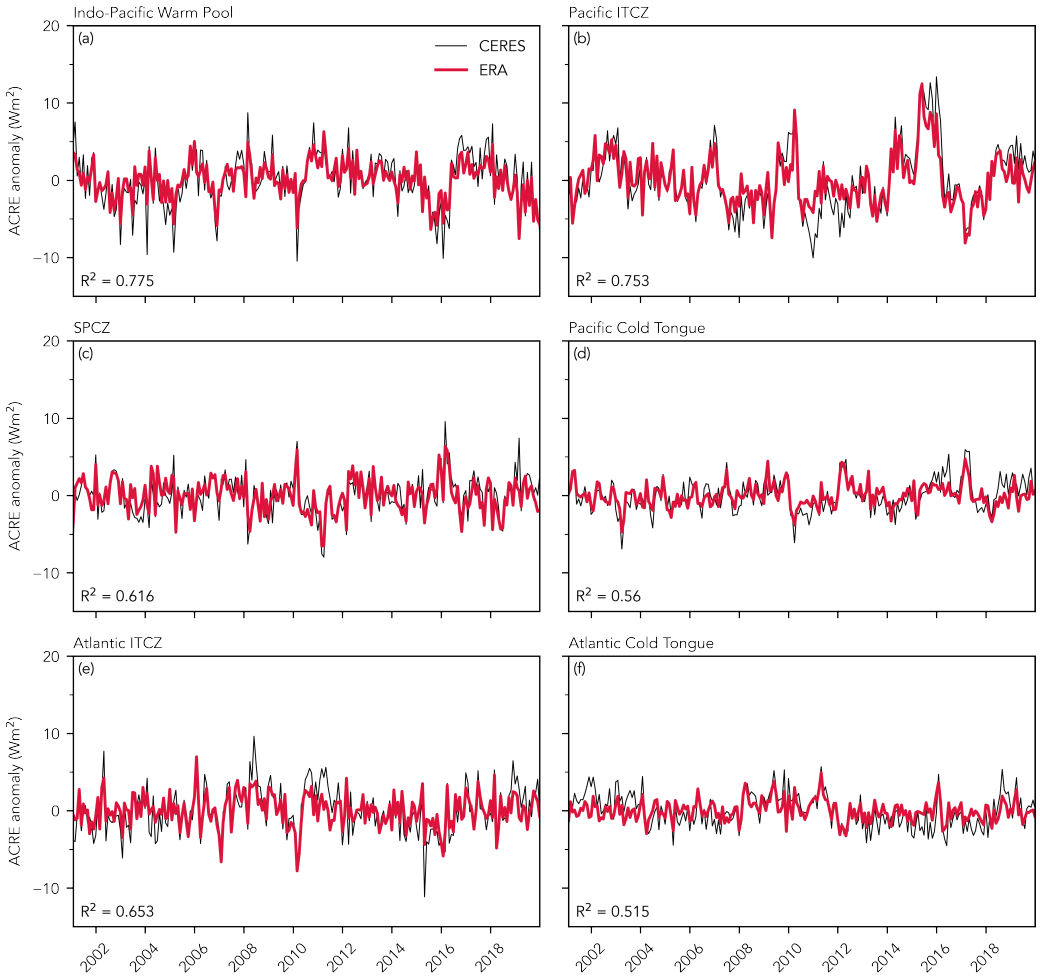

Figure 3. **(a)** De-seasonalized time series of monthly mean ACRE anomaly averaged over the Indo-Pacific warm pool. Black line shows the ACRE anomaly observed from CERES satellite fluxes, while the red line shows the ACRE anomaly estimated from ERA5. **(b)-(f):** same as **(a)**, but averaged over, respectively, the pacific ITCZ, the SPCZ, the Pacific cold tongue, the Atlantic ITCZ, and the Atlantic cold tongue. Outlines of the six regions are shown as boxes in Fig. 1 Each r leading to the calculation of an R^2 is significant at the 0.05 level.

50% of the variance of the ACRE on monthly time scales can be explained by the CRH in each of these regions.

The R^2 correlations for the monthly mean time series are recorded in Tbl. S1, alongside the R^2 correlations for the daily mean time series, which were constructed in much the same way. On daily time scales the agreement is lower than monthly time scales, although the correlation is still greater than 0.6 in the warm pool, and greater than 0.4 in all regions except for the Pacific cold tongue. From this, it appears that the CRH method is shows some skill at estimating the ACRE even on time scales shorter than a month.

4.3 Discussion

What accounts for this relationship between CRH and the ACRE? We believe that the explanation lies in the curves in Figs. 1.c and 1.d, which show that precipitation and ACRE depend on CRH in a similar way. Both are small when the CRH is small, and both increase rapidly when the CRH exceeds a critical threshold. We suggest that this similarity is more than just coincidence, and that the dependence of precipitation on CRH is linked to the ACRE because of cloud-longwave feedbacks which have been recently identified in the context of organized tropical systems.

In a companion paper, Needham and Randall (2021) discuss this type of feedback in the context of a set of idealized simulations. They find that the ACRE in extremely humid regions is powerful enough to change the sign of the net radiation tendency, which leads to an atmospheric energy convergence. The net heating drives stratiform ascent which lifts water vapor and moistens the troposphere (Chikira, 2014; Ahmed & Schumacher, 2015; Jenney et al., 2020). Through mass continuity the ascent leads to low-level convergence which transports water vapor into regions that are already quite humid (Riehl & Malkus, 1958; Neelin & Held, 1987), which provides moisture to continue the feedback.

We argue that the exponential dependence of the precipitation rate on the CRH is a result of this cloud-longwave feedback. The ascent driven by ACRE favors a shift from isolated convection to more organized systems that are characterized by stratiform precipitation. As discussed by Ahmed and Schumacher (2015), the area covered by stratiform precipitation increases exponentially at high CRH, and accounts for the characteristic pickup of the precipitation rate above the critical threshold.

5 Conclusions

We have shown that the ACRE varies with the CRH in a way that is similar to the well-documented relationship between precipitation and CRH. When the ACRE from $1° \times 1°$ daily mean satellite observations is binned by the CRH, the net ACRE increases rapidly above a critical threshold, with very little spread in the distribution of ACRE at a particular CRH. This suggests that the ACRE can be estimated from the CRH, in the same way that CRH has been used to estimate precipitation. Our estimation method is able to reproduce the large-scale annual mean spatial distribution of ACRE in the tropics, which includes a well defined ITCZ and Indo-Pacific warm pool. The difference in the observed and estimated ACRE is 0.01 W m^{-2} averaged over the domain, due to positive and negative errors which mostly cancel. Comparisons of the observed and estimated regional time series of ACRE show a high degree of agreement on monthly time scales, with slightly less agreement on daily time scales. The method is also able to reproduce large peaks in the magnitude of the ACRE in the ITCZ and warm pool regions associated with ENSO variability. Generally the method works better in regions associated with deep convective clouds, compared to the cold tongue regions that are characterized by marine stratus clouds.

An explanation for the exponential relationship between precipitation and CRH is proposed in the form of a moisture feedback driven by ACRE. Cloud-longwave heating leads to stratiform rising motion and moisture convergence, which in turn lead to the formation of more clouds. The rising motion coincides with a shift from convective to stratiform precipitation, which has been identified as a key component of the non-linear relationship between precipitation and CRH. This and other aspects of tropical cloud-longwave feedbacks are discussed further in a companion paper.

Acknowledgments

We would like to thank two anonymous reviewers for helpful comments on an earlier version of this manuscript. This research has been partially funded by the National Science Foundation.

Open Research

All of the data used in this study are freely available online. ERA5 reanalysis data were downloaded from the ECMWF Copernicus Climate Data Store (CDS), accessible at `https://cds.climate.copernicus.eu/`. CERES SYN1deg_Ed4a data were obtained from the NASA Langley Research Center Atmospheric Science Data Center (ASDC), accessible at `https://ceres.larc.nasa.gov/`. TRMM data were downloaded from the Goddard Earth Sciences Data and Information Services Center (GES DISC), accessible at `https://disc.gsfc.nasa.gov/`.

References

Ahmed, F., & Schumacher, C. (2015, December). Convective and stratiform components of the precipitation-moisture relationship. *Geophys. Res. Lett.*, *42*(23). Retrieved from `https://onlinelibrary.wiley.com/doi/abs/10.1002/2015GL066957` doi: 10.1002/2015gl066957

Albern, N., Voigt, A., Buehler, S. A., & Grützun, V. (2018, August). Robust and nonrobust impacts of atmospheric Cloud-Radiative interactions on the tropical circulation and its response to surface warming. *Geophys. Res. Lett.*, *27*, 4937. Retrieved from `http://doi.wiley.com/10.1029/2018GL079599` doi: 10.1029/2018GL079599

Allan, R. P. (2011, September). Combining satellite data and models to estimate cloud radiative effect at the surface and in the atmosphere. *Met. Apps*, *18*(3), 324-333. doi: 10.1002/met.285

Arnold, N. P., & Randall, D. A. (2015, December). Global-scale convective aggregation: Implications for the Madden-Julian oscillation: GLOBAL-SCALE CONVECTIVE AGGREGATION. *J. Adv. Model. Earth Syst.*, *7*(4), 1499-1518. Retrieved from `http://doi.wiley.com/10.1002/2015MS000498` doi: 10.1002/2015ms000498

Benedict, J. J., Medeiros, B., Clement, A. C., & Olson, J. G. (2020, May). Investigating the role of cloud-radiation interactions in subseasonal tropical disturbances. *Geophys. Res. Lett.*, *47*(9), e2019GL086817. Retrieved from `https://onlinelibrary.wiley.com/doi/10.1029/2019GL086817` doi: 10.1029/2019gl086817

Bretherton, C. S., Blossey, P. N., & Khairoutdinov, M. (2005, December). An

Energy-Balance analysis of deep convective Self-Aggregation above uniform SST. *J. Atmos. Sci.*, *62*(12), 4273-4292. Retrieved from https://doi.org/10.1175/JAS3614.1 doi: 10.1175/JAS3614.1

Bretherton, C. S., Peters, M. E., & Back, L. E. (2004). Relationships between water vapor path and precipitation over the tropical oceans. *J. Clim.*, *17*(7), 1517-1528.

Chikira, M. (2014, February). Eastward-Propagating intraseasonal oscillation represented by Chikira–Sugiyama cumulus parameterization. part II: Understanding moisture variation under weak temperature gradient balance. *J. Atmos. Sci.*, *71*(2), 615-639. Retrieved from https://journals.ametsoc.org/jas/article/71/2/615/27839/Eastward-Propagating-Intraseasonal-Oscillation doi: 10.1175/JAS-D-13-038.1

Dixit, V., Geoffroy, O., & Sherwood, S. C. (2018, June). Control of ITCZ width by low-level radiative heating from upper-level clouds in aquaplanet simulations. *Geophys. Res. Lett.*, *45*(11), 5788-5797. Retrieved from https://onlinelibrary.wiley.com/doi/abs/10.1029/2018GL078292 doi: 10.1029/2018gl078292

Doelling, D. R., Loeb, N. G., Keyes, D. F., Nordeen, M. L., Morstad, D., Nguyen, C., … Sun, M. (2013, June). Geostationary enhanced temporal interpolation for CERES flux products. *J. Atmos. Ocean. Technol.*, *30*(6), 1072-1090. Retrieved from https://journals.ametsoc.org/view/journals/atot/30/6/jtech-d-12-00136_1.xml doi: 10.1175/JTECH-D-12-00136.1

Emanuel, K. (2019, January). Inferences from simple models of slow, convectively coupled processes. *J. Atmos. Sci.*, *76*(1), 195-208. Retrieved from https://doi.org/10.1175/JAS-D-18-0090.1 doi: 10.1175/JAS-D-18-0090.1

Harrop, B. E., & Hartmann, D. L. (2016, April). The role of cloud radiative heating in determining the location of the ITCZ in aquaplanet simulations. *J. Clim.*, *29*(8), 2741-2763. doi: 10.1175/JCLI-D-15-0521.1

Hersbach, H., Bell, B., Berrisford, P., Biavati, G., Horányi, A., Muñoz Sabater, J., … Thépaut, J.-N. (2018). *ERA5 hourly data on pressure levels from 1979 to present.* Retrieved from http://dx.doi.org/10.24381/cds.bd0915c6 doi: 10.24381/cds.bd0915c6

Hersbach, H., Bell, B., Berrisford, P., Hirahara, S., Horányi, A., Muñoz-Sabater, J.,

… Thépaut, J. (2020, July). The ERA5 global reanalysis. *Q.J.R. Meteorol. Soc.*, *146*(730), 1999-2049. Retrieved from https://onlinelibrary.wiley.com/doi/abs/10.1002/qj.3803 doi: 10.1002/qj.3803

Huffman, G. J., Bolvin, D. T., Nelkin, E. J., & Adler, R. F. (2016). *TRMM (TMPA) precipitation L3 1 day 0.25 degree x 0.25 degree V7 (TRMM_3B42_Daily).* Retrieved from https://disc.gsfc.nasa.gov/datasets/TRMM_3B42_Daily_7/summary doi: 10.5067/TRMM/TMPA/DAY/7

Jenney, A. M., Randall, D. A., & Branson, M. D. (2020, May). Understanding the response of tropical ascent to warming using an energy balance framework. *J. Adv. Model. Earth Syst.*. Retrieved from https://onlinelibrary.wiley.com/doi/abs/10.1029/2020MS002056 doi: 10.1029/2020MS002056

Khairoutdinov, M. F., & Emanuel, K. (2018, December). Intraseasonal variability in a Cloud-Permitting Near-Global equatorial aquaplanet model. *J. Atmos. Sci.*, *75*(12), 4337-4355. Retrieved from https://journals.ametsoc.org/view/journals/atsc/75/12/jas-d-18-0152.1.xml doi: 10.1175/JAS-D-18-0152.1

Klein, S. A., & Hartmann, D. L. (1993, August). The seasonal cycle of low stratiform clouds. *J. Clim.*, *6*(8), 1587-1606. doi: 10.1175/1520-0442(1993)006<1587:TSCOLS>2.0.CO;2

Kubar, T. L., Hartmann, D. L., & Wood, R. (2007, November). Radiative and convective driving of tropical high clouds. *J. Clim.*, *20*(22), 5510-5526. doi: 10.1175/2007JCLI1628.1

Li, Y., Thompson, D. W. J., & Bony, S. (2015, September). The influence of atmospheric cloud radiative effects on the Large-Scale atmospheric circulation. *J. Clim.*, *28*(18), 7263-7278. Retrieved from https://journals.ametsoc.org/view/journals/clim/28/18/jcli-d-14-00825.1.xml?tab_body=pdf doi: 10.1175/JCLI-D-14-00825.1

Medeiros, B., Clement, A. C., Benedict, J. J., & Zhang, B. (2021, March). Investigating the impact of cloud-radiative feedbacks on tropical precipitation extremes. *npj Climate and Atmospheric Science*, *4*(1), 1-10. Retrieved from https://www.nature.com/articles/s41612-021-00174-x doi: 10.1038/s41612-021-00174-x

National Weather Service. (2020, December). *Cold & warm episodes by season.*

https://origin.cpc.ncep.noaa.gov/products/analysis_monitoring/ensostuff/ONI_v5.php. Retrieved from https://origin.cpc.ncep.noaa.gov/products/analysis_monitoring/ensostuff/ONI_v5.php (Accessed: 2020-12-22)

Needham, M. R., & Randall, D. A. (2021, April). *Riehl and malkus revisited: The role of Cloud-Radiative effects.* Retrieved from https://www.essoar.org/doi/abs/10.1002/essoar.10506726.1

Neelin, J. D., & Held, I. M. (1987). Modeling tropical convergence based on the moist static energy budget. *Mon. Weather Rev.*, *115*(1), 3–12.

Popp, M., & Silvers, L. G. (2017, November). Double and single ITCZs with and without clouds. *J. Clim.*, *30*(22), 9147-9166. doi: 10.1175/JCLI-D-17-0062.1

Powell, S. W. (2019, December). Observing possible thermodynamic controls on tropical marine rainfall in moist environments. *J. Atmos. Sci.*, *76*(12), 3737-3751. doi: 10.1175/jas-d-19-0144.1

Ramanathan, V. (1987). The role of earth radiation budget studies in climate and general circulation research. *J. Geophys. Res.*, *92*(D4), 4075. doi: 10.1029/JD092iD04p04075

Randall, D. A., Harshvardhan, Dazlich, D. A., & Corsetti, T. G. (1989, July). Interactions among radiation, convection, and Large-Scale dynamics in a general circulation model. *J. Atmos. Sci.*, *46*(13), 1943-1970. Retrieved from https://journals.ametsoc.org/jas/article/46/13/1943/22282/Interactions-among-Radiation-Convection-and-Large doi: 10.1175/1520-0469(1989)046<1943:IARCAL>2.0.CO;2

Raymond, D. J. (2000, July). Thermodynamic control of tropical rainfall. *Q.J.R. Meteorol. Soc.*, *126*(564), 889-898. doi: 10.1002/qj.49712656406

Raymond, D. J., Sessions, S. L., Sobel, A. H., & Fuchs, Ž. (2009, March). The mechanics of gross moist stability. *J. Adv. Model. Earth Syst.*, *1*(3). doi: 10.3894/JAMES.2009.1.9

Raymond, D. J., & Zeng, X. (2005, April). Modelling tropical atmospheric convection in the context of the weak temperature gradient approximation. *Quart. J. Roy. Meteor. Soc.*, *131*(608), 1301-1320. doi: 10.1256/qj.03.97

Riehl, H., & Malkus, J. S. (1958). On the heat balance in the equatorial trough zone. *Geophysica*, *6*, 503-537.

Ruppert, J. H., Jr, Wing, A. A., Tang, X., & Duran, E. L. (2020, November). The critical role of cloud-infrared radiation feedback in tropical cyclone development. *Proc. Natl. Acad. Sci. U. S. A.*, *117*(45), 27884-27892. Retrieved from http://dx.doi.org/10.1073/pnas.2013584117 doi: 10.1073/pnas.2013584117

Rushley, S. S., Kim, D., Bretherton, C. S., & Ahn, M.-S. (2018, January). Re-examining the non-linear moisture-precipitation relationship over the tropical oceans. *Geophys. Res. Lett.*, *45*(2), 1133-1140. doi: 10.1002/2017GL076296

Sherwood, S. C., Ramanathan, V., Barnett, T. P., Tyree, M. K., & Roeckner, E. (1994). Response of an atmospheric general circulation model to radiative forcing of tropical clouds. *J. Geophys. Res.*, *99*(D10), 20829. doi: 10.1029/94jd01632

Slingo, A., & Slingo, J. M. (1988, July). The response of a general circulation model to cloud longwave radiative forcing. i: Introduction and initial experiments. *Q.J Royal Met. Soc.*, *114*(482), 1027-1062. doi: 10.1002/qj.49711448209

Stevens, B., Bony, S., & Webb, M. (2012, September). *CLOUDS ON-OFF KLIMATE INTERCOMPARISON EXPERIMENT (COOKIE).* http://www.euclipse.eu/wp4/wp4.html. Retrieved from http://www.euclipse.eu/wp4/wp4.html (Accessed: 2020-7-28)

Voigt, A., & Albern, N. (2019, December). No cookie for climate change. *Geophys. Res. Lett.*, *46*(24), 14751-14761. Retrieved from https://onlinelibrary.wiley.com/doi/abs/10.1029/2019GL084987 doi: 10.1029/2019GL084987

Wing, A. A., Emanuel, K., Holloway, C. E., & Muller, C. (2017, November). Convective Self-Aggregation in numerical simulations: A review. *Surv. Geophys.*, *38*(6), 1173-1197. doi: 10.1007/s10712-017-9408-4

Wolding, B., Dias, J., Kiladis, G., Ahmed, F., Powell, S. W., Maloney, E., & Branson, M. (2020, May). Interactions between moisture and tropical convection. part i: The coevolution of moisture and convection. *J. Atmos. Sci.*, *77*(5), 1783-1799. doi: 10.1175/jas-d-19-0225.1

Wolding, B., Maloney, E. D., & Branson, M. (2016, December). Vertically resolved weak temperature gradient analysis of the Madden-Julian oscillation in SP-CESM. *J. Adv. Model. Earth Syst.*, *8*(4), 1586-1619. Retrieved from https://onlinelibrary.wiley.com/doi/abs/10.1002/2016MS000724 doi:

10.1002/2016ms000724

Yoneyama, K., Zhang, C., & Long, C. N. (2013, December). Tracking pulses of the Madden–Julian oscillation. *Bull. Am. Meteorol. Soc.*, *94*(12), 1871-1891. Retrieved from `https://journals.ametsoc.org/view/journals/bams/94/12/bams-d-12-00157.1.xml` doi: 10.1175/BAMS-D-12-00157.1

Zeng, X. (1999, August). The relationship among precipitation, Cloud-Top temperature, and precipitable water over the tropics. *J. Clim.*, *12*(8), 2503-2514. Retrieved from `https://journals.ametsoc.org/view/journals/clim/12/8/1520-0442_1999_012_2503_trapct_2.0.co_2.xml` doi: 10.1175/1520-0442(1999)012<2503:TRAPCT>2.0.CO;2

Supporting Information for "Linking Atmospheric Cloud Radiative Effects and Tropical Precipitation"

Michael R. Needham[1]and David A. Randall[1]

[1]Colorado State University

Contents of this file

1. Text S1 to S3
2. Figures S1 to S9
3. Table S1

Text S1: Regions of the Tropics and Distributions of CRH

The latitude and longitude boundaries for the six tropical regions used in the main text are recorded in Tbl. S1. The regions were selected to give a range of underlying sea surface temperature (SST) and column relative humidity (CRH) distributions (see Fig. S1). The Indo-Pacific warm pool, south Pacific convergence zone, Pacific ITCZ and Atlantic ITCZ regions are characterized by time-mean low-level moisture convergence which favors deep convection. In contrast, the Atlantic and Pacific cold tongue regions are characterized by

Corresponding author: Michael R. Needham, Department of Atmospheric Science, Colorado State University, Fort Collins, CO, 80521, USA. (m.needham@colostate.edu)

cold upwelling SSTs and are situated under the descending branch of the Hadley cells. The cold SSTs and subsiding motion both tend to suppresses deep convection and favor the formation of marine stratocumulus clouds.

Probability density functions (PDFs) of column relative humidity (CRH) are included in the six panels of Fig. S1. The CRH appears to follow a bimodal distribution, with a "humid peak" near 80% and a "dry peak" near 40%. The Indo-Pacific and ITCZ regions have a single mode near the humid peak, while the cold tongue regions have a single moad near the dry peak. Only the SPCZ region exhibits the bimodal behavior of the wider tropical belt.

Text S2: ACRE Binned by CRH for Six Tropical Regions

Fig. S2 shows the net ACRE binned by the CRH for the six regions specified in the main text and in Tbl. S1. Each panel shows a rapid increase in magnitude above a threshold of about 60%. This is consistent with the curve of the ACRE vs. CRH over the entire tropical belt from 30°S to 30°N (see Fig. 1.d in the main text).

As mentioned in the main text, the curves for the cold tongue regions (Fig. S2.e and S2.f) each show the influence of marine stratus clouds. These clouds occur in relatively dry conditions under the subsiding branches of the hadley cells. Because they are bright, they reflect a large amount of solar radiation and have a large negative ACRE. This is illustrated in Fig. S2.e and S2.f as the, negative extrema near 20$ CRH that is absent in the other panels. This likely contributes to the error in the estimation method in these regions (Fig. S2 of the main text).

Text S3: Composite ENSO Analysis of Estimated ACRE

The time series analysis of the main text (Fig. 3) suggests that the estimation method may be more biased in the Pacific ITCZ, Indo-Pacific Warm Pool or Pacific cold tongue regions during different phases of ENSO variability.

To investigate this, we repeat the calculation of Pearson's R^2 correlation for each of the six regions, composited by ENSO phase. We use the Oceanic Niño Index (ONI, National Weather Service (2020)) as our metric for ENSO phase. An El Niño occurs when the ONI exceeds 0.5 K for 5 consecutive months, while a La Niña occurs when the ONI is less than -0.5 for 5 consecutive months. Fig. S3 shows a time series of the ONI aligned with the 19-year period used in the main texts. El Niño (La Niña) periods are colored red (blue). For the sake of completeness the analysis is repeated for each of the six regions (Figs. S4 through S9), but we focus only on the Pacific ITCZ (Fig. S4) and Indo-Pacific warm pool (Fig. S5), which show the most clear dependence on ENSO.

The top left panel of Fig. S4 shows the correlation between the estimated (y-axis) and observed (x-axis) monthly ACRE anomalies in the Pacific ITCZ region, with data points colored according to the ENSO phase. A first look shows a relationship between ENSO phase as ACRE anomaly in this region: El Niño conditions (red) support enhanced convection due to warmer SSTs in the eastern equatorial Pacific, leading to positive ACRE anomalies, while La Niña conditions (blue) suppress convection due to cooler SSTs, leading to negative anomalies. In the Indo-Pacific regions (Fig. S5), the opposite occurs. In this region, El Niño is associated with *cooler* SSTs, while La Niña is associated with *warmer* SSTs. The result is that El Niño (red) months in Fig. S5 are associated with

negative ACRE anomalies, and La Niña (blue) months are associated with positive ACRE anomalies.

The R^2 correlation is 0.401 during La Niña in the Pacific ITCZ, while it is above 0.7 during the neutral and Niño phases in that region (bottom row of Fig. S4). This suggests that the estimation method is less accurate in this region during La Niña due to a lower frequency of organized convection at the expense of marine stratus clouds. The R^2 correlations do not seem to vary with ENSO in the Indo-Pacific region, or in any of the other regions. There is a slight difference in the Atlantic Cold Tongue region, but this is likely due to noise, as the anomalies all centered around zero during each ENSO phase (Bottom row of Fig. S9)

References

National Weather Service. (2020, December). *Cold & warm episodes by season.* `https://origin.cpc.ncep.noaa.gov/products/analysis_monitoring/ensostuff/ONI_v5.php`. Retrieved from `https://origin.cpc.ncep.noaa.gov/products/analysis_monitoring/ensostuff/ONI_v5.php` (Accessed: 2020-12-22)

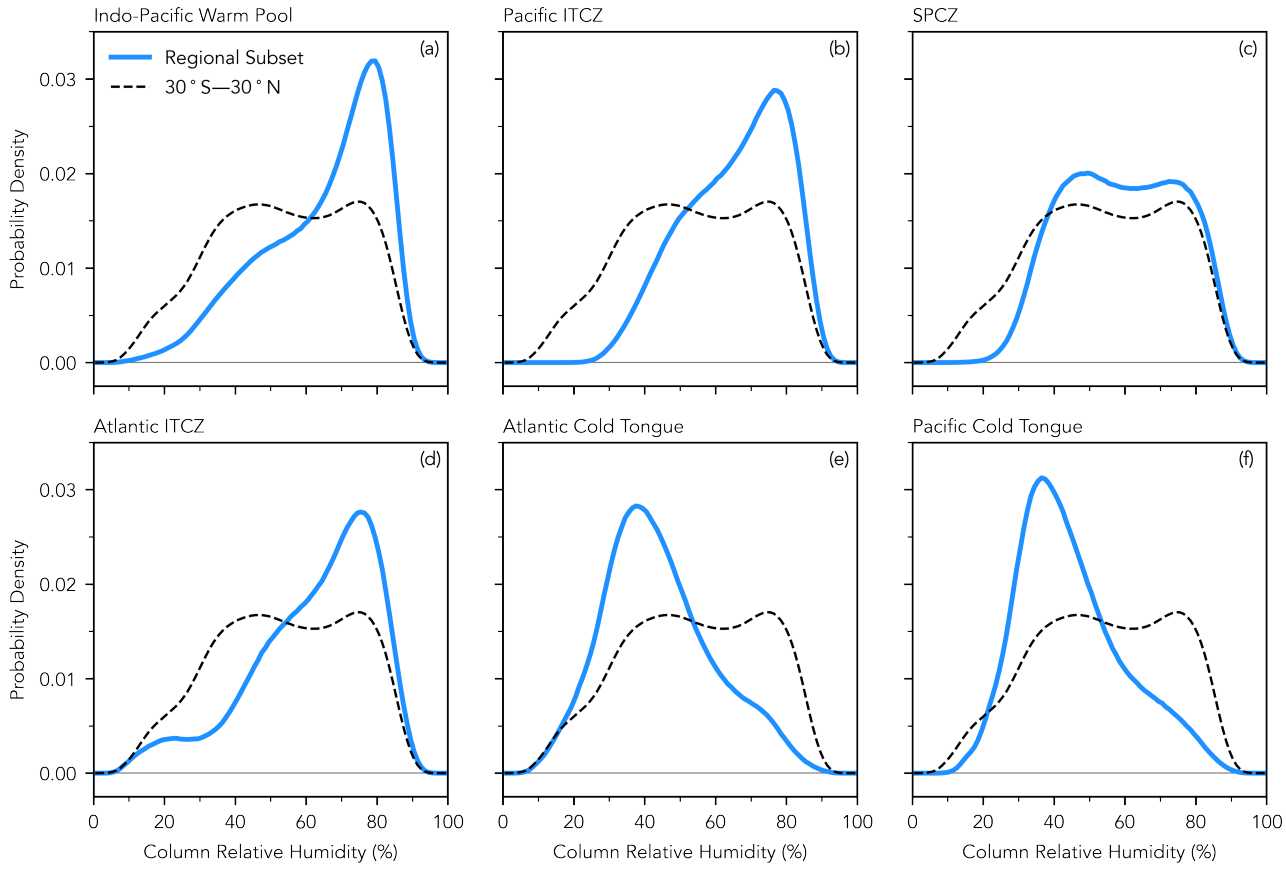

Figure S1. **(a)** Probability density functions of column relative humidity for the Indo-Pacific warm pool (red line) and over the entire 30°S-30°N tropical belt. **(b)-(f):** same as **(a)**, but for, respectively, the pacific ITCZ, the SPCZ, the Pacific cold tongue, the Atlantic ITCZ, and the Atlantic cold tongue.

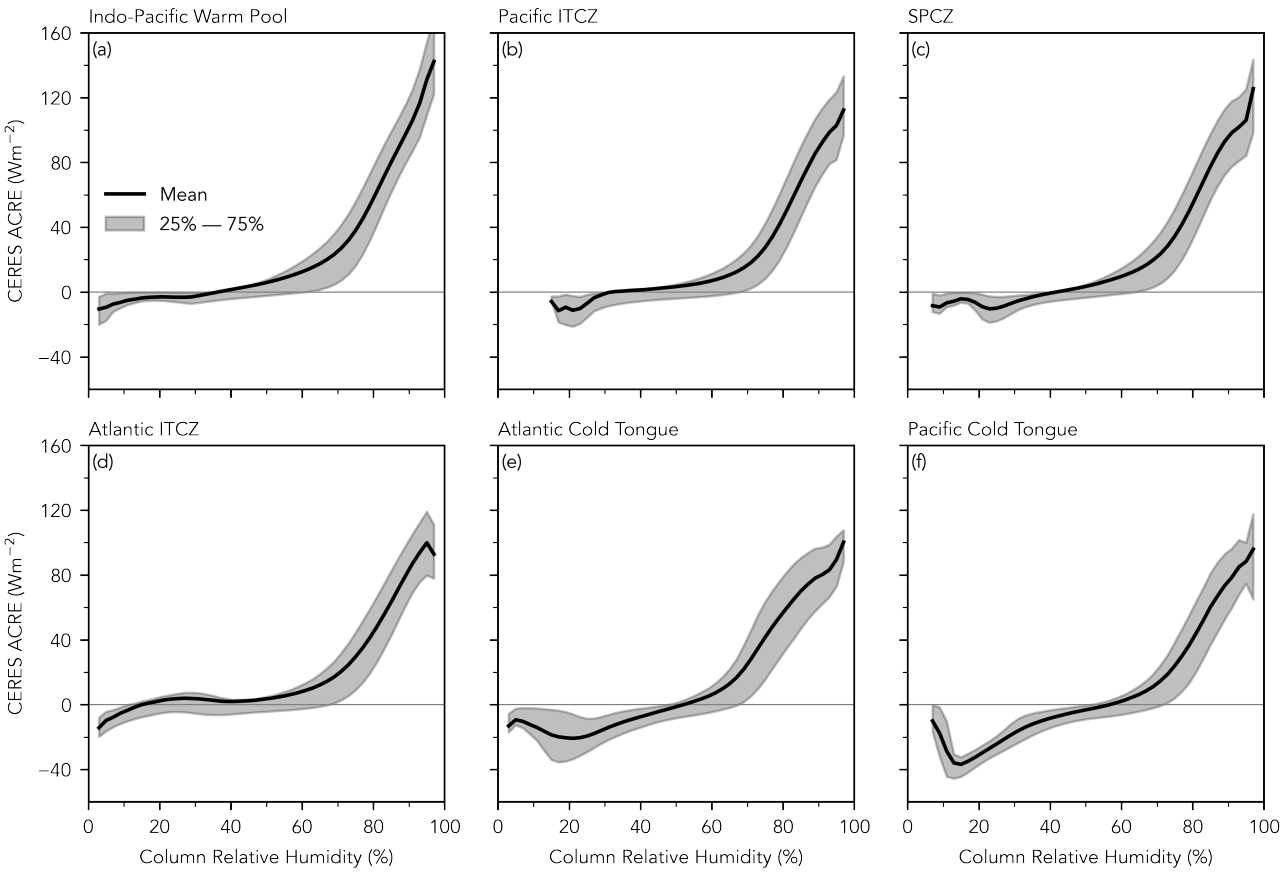

Figure S2. Net (longwave plus shortwave) ACRE binned by the CRH for the six tropical regions specified in Fig. 1.a of the main text.

Table S1. Pearson's R^2 correlation between ACRE calculated from CERES observations and ACRE estimated from ERA5 CRH at monthly and daily time-scales for each of the six tropical sub regions. Also included are the latitude and longitude boundaries for each region.

	Regional Extent	Monthly R^2	Daily R^2
Indo-Pacific Warm Pool	70°E-170°W, 20°S-20°N	0.775	0.624
Pacific ITCZ	150°E-100°W, 0°-15°N	0.753	0.569
SPCZ	150°E-130°W, 30°S-0°	0.616	0.486
Pacific Cold Tongue	130°W-95°W, 30°S-0°	0.56	0.39
Atlantic ITCZ	55°W-15°E, 5°S-15°N	0.653	0.507
Atlantic Cold Tongue	40°W-20°E, 30°S-5°N	0.515	0.421

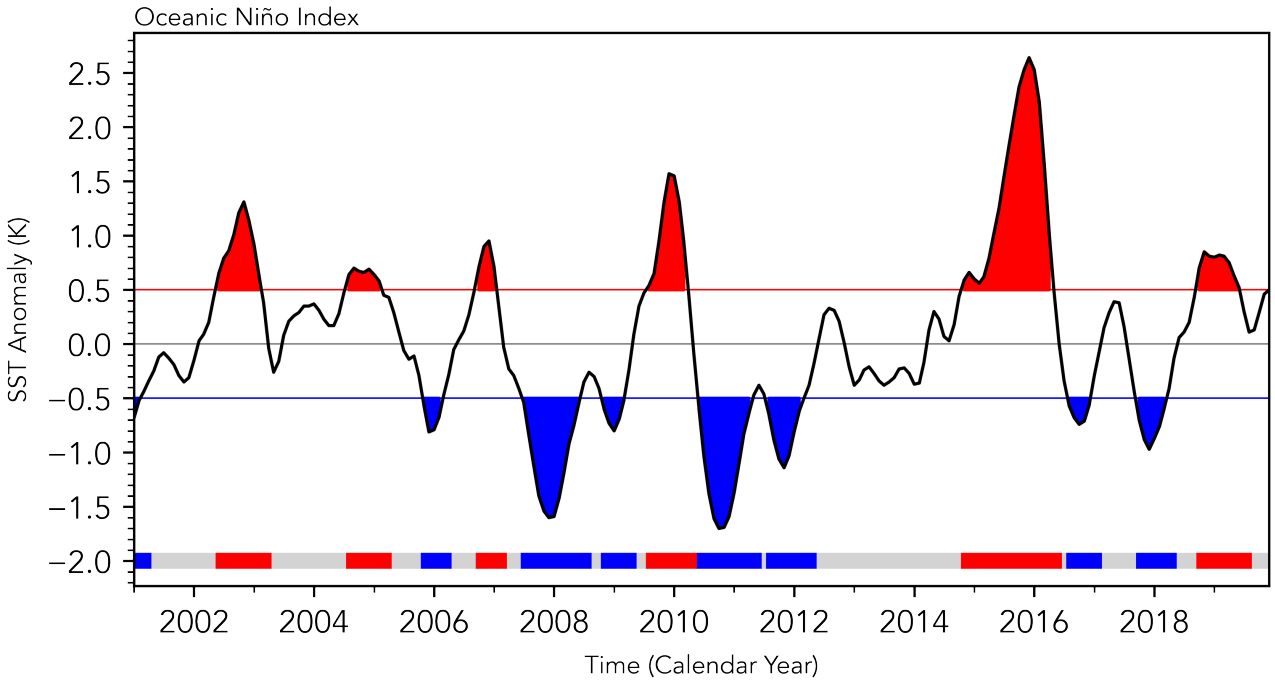

Figure S3. Oceanic Niño index, showing centered, 3-month running average SST anomaly over the Ni no 3.4 region of the eastern Pacific.

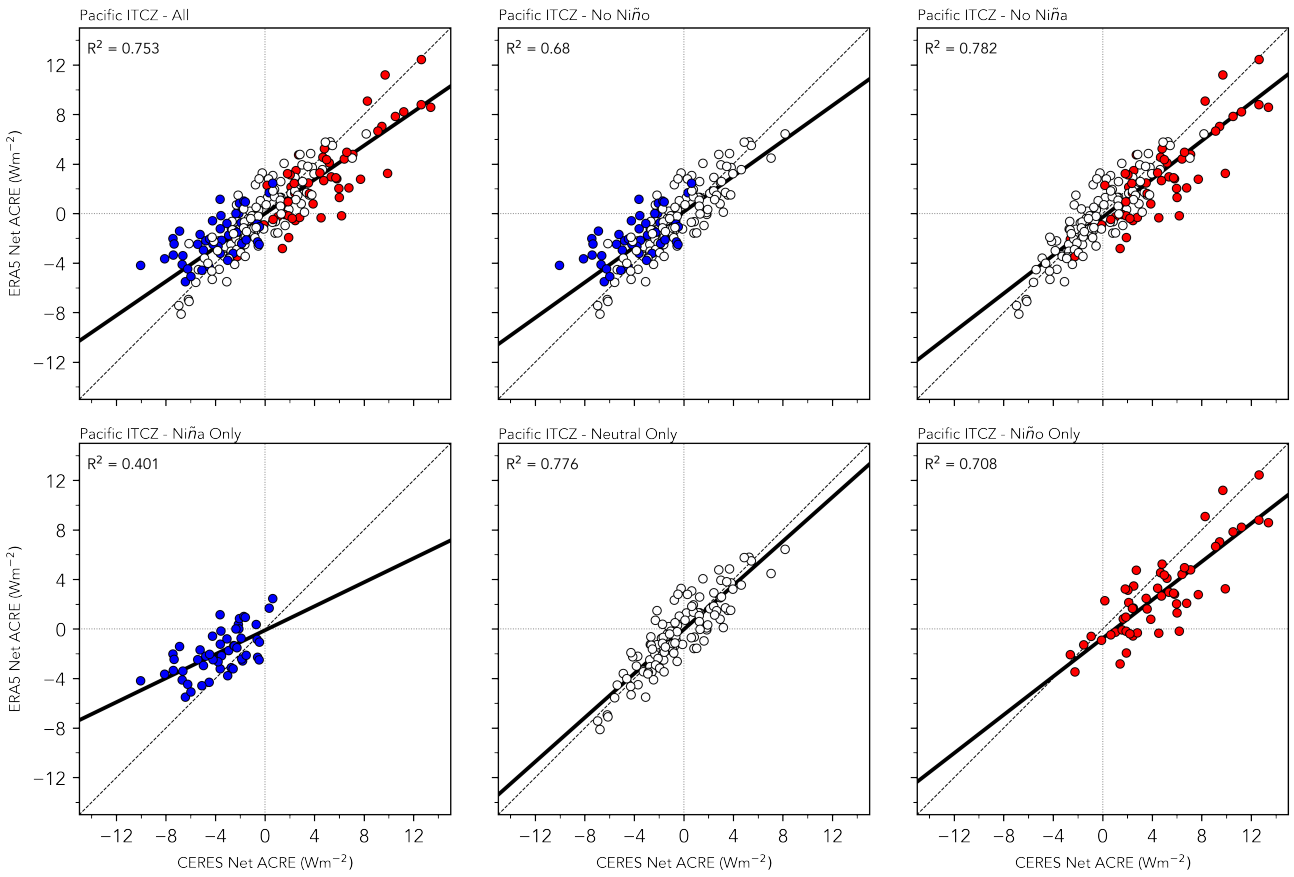

Figure S4. Correlation between ACRE observed from CERES fluxes (horizontal) with ACRE estimated from ERA5 CRH for the Pacific ITCZ region, as described in the main text. The color of the dots in each panel indicates the ONI phase (See Fig. S3) associated with each data point: red indicates El Niño, white indicates neutral, and blue indicates La Niña. **Top Left:** Correlation for all months. **Top Center:** Correlation for neutral and Niña. months only. **Top Right:** Correlation for Niño and neutral months only. **Bottom Left:** Correlation for Niña months only. **Bottom Center:** Correlation for neutral months only. **Bottom Right:** Correlation for Niño months only. In each panel, the thick black line shows the line of best fit (least-squares regression), and the dashed diagonal line shows a perfect one-to-one correlation.

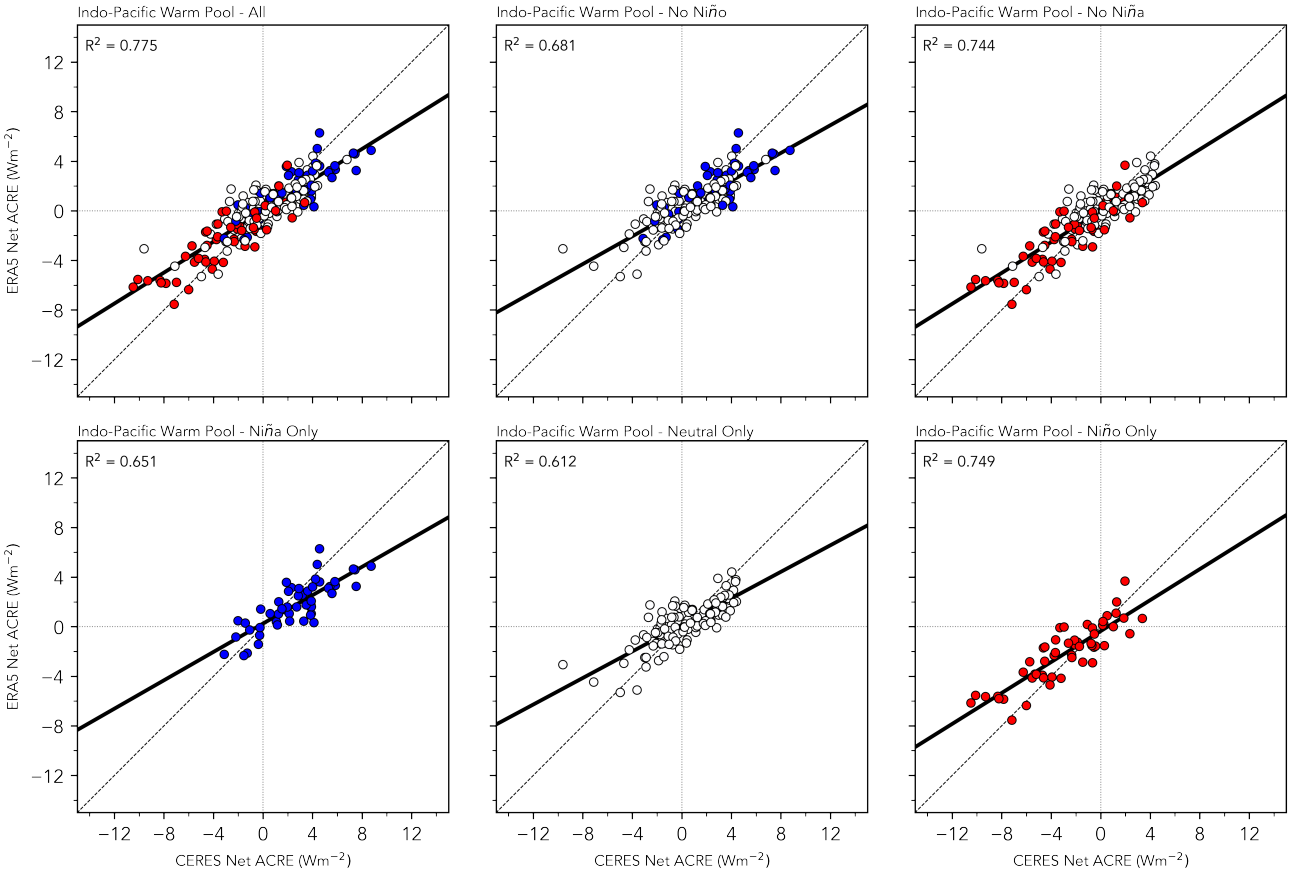

Figure S5. Same as Fig. S4, but for the Indo-Pacific Warm Pool

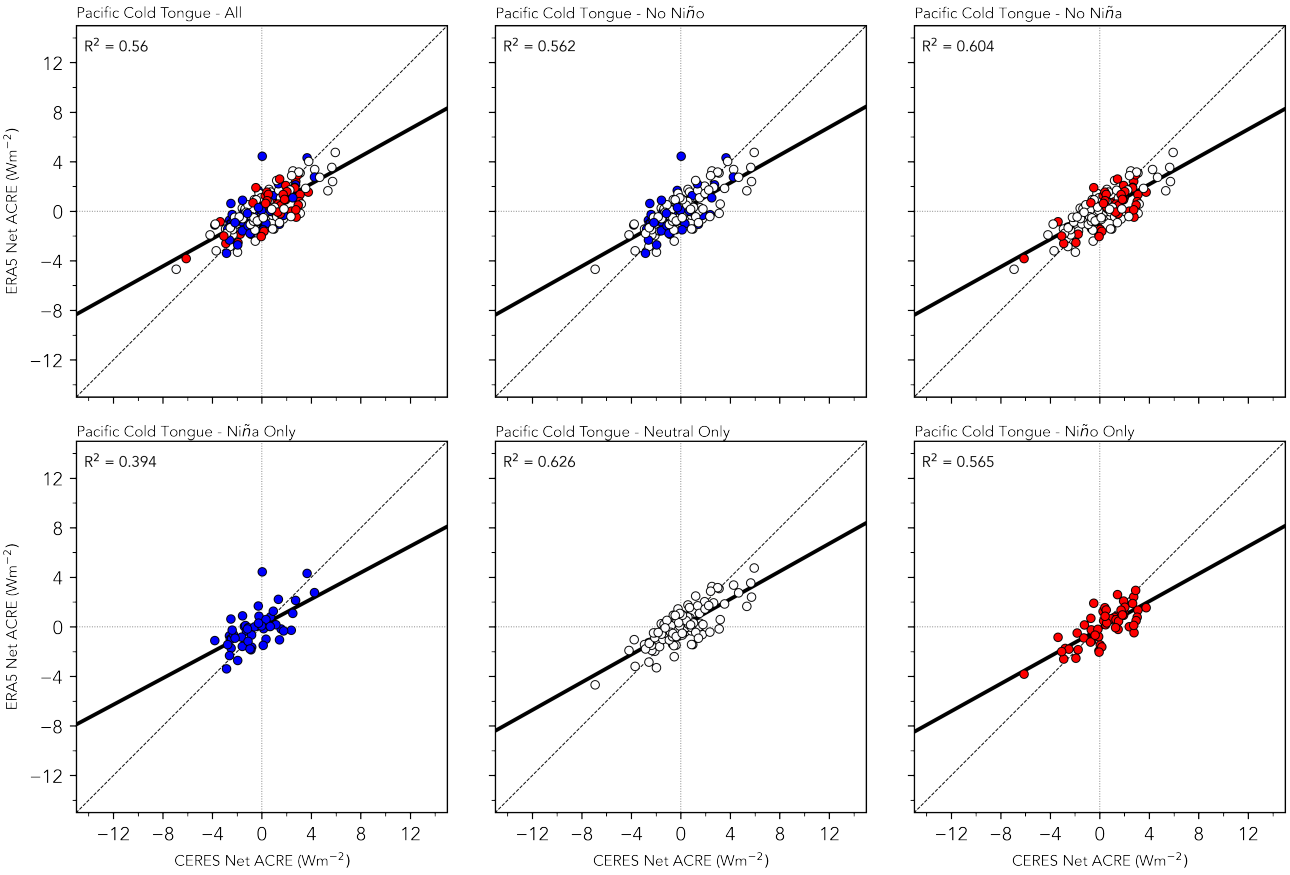

Figure S6. Same as Fig. S4, but for the Pacific cold tongue

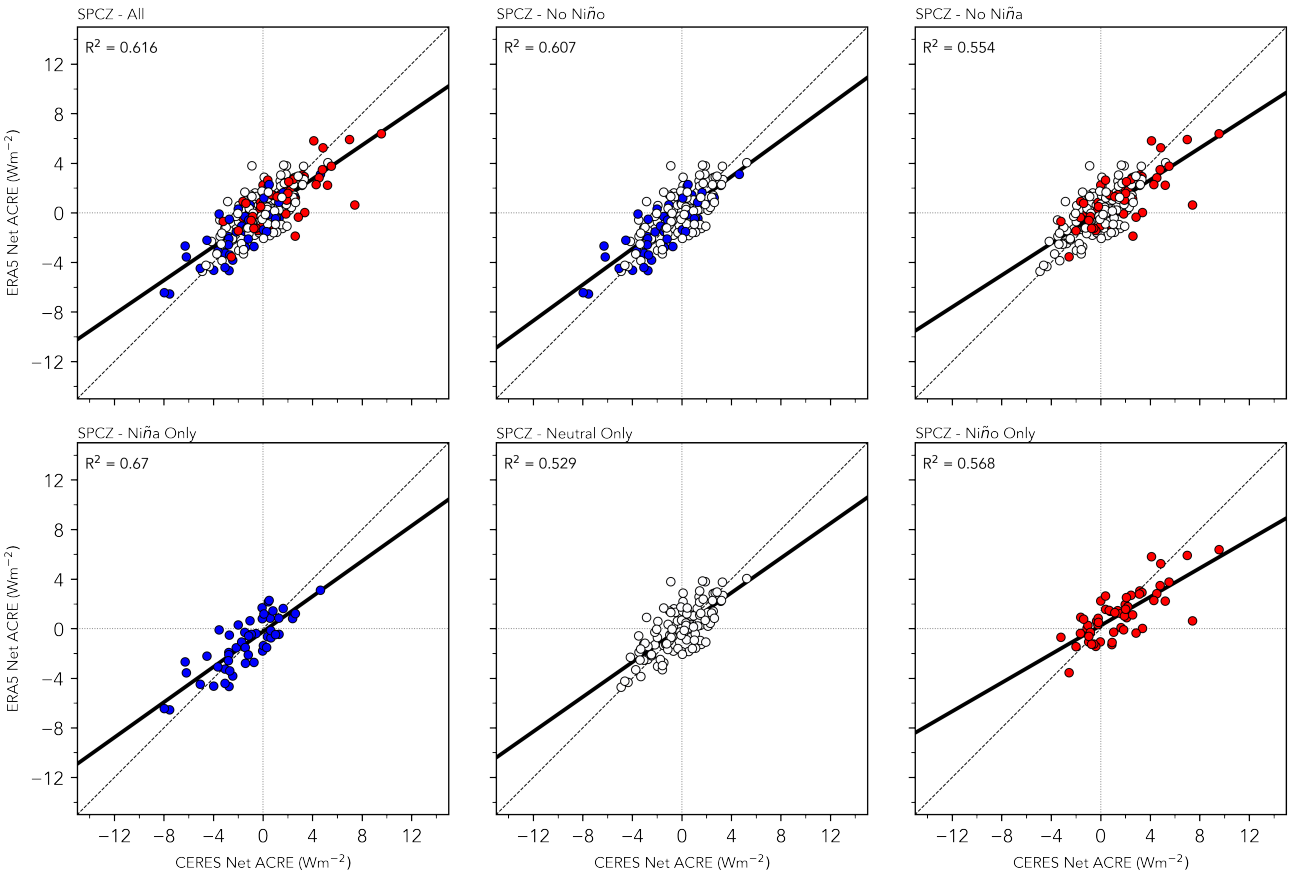

Figure S7. Same as Fig. S4, but for the Atlantic ITCZ region

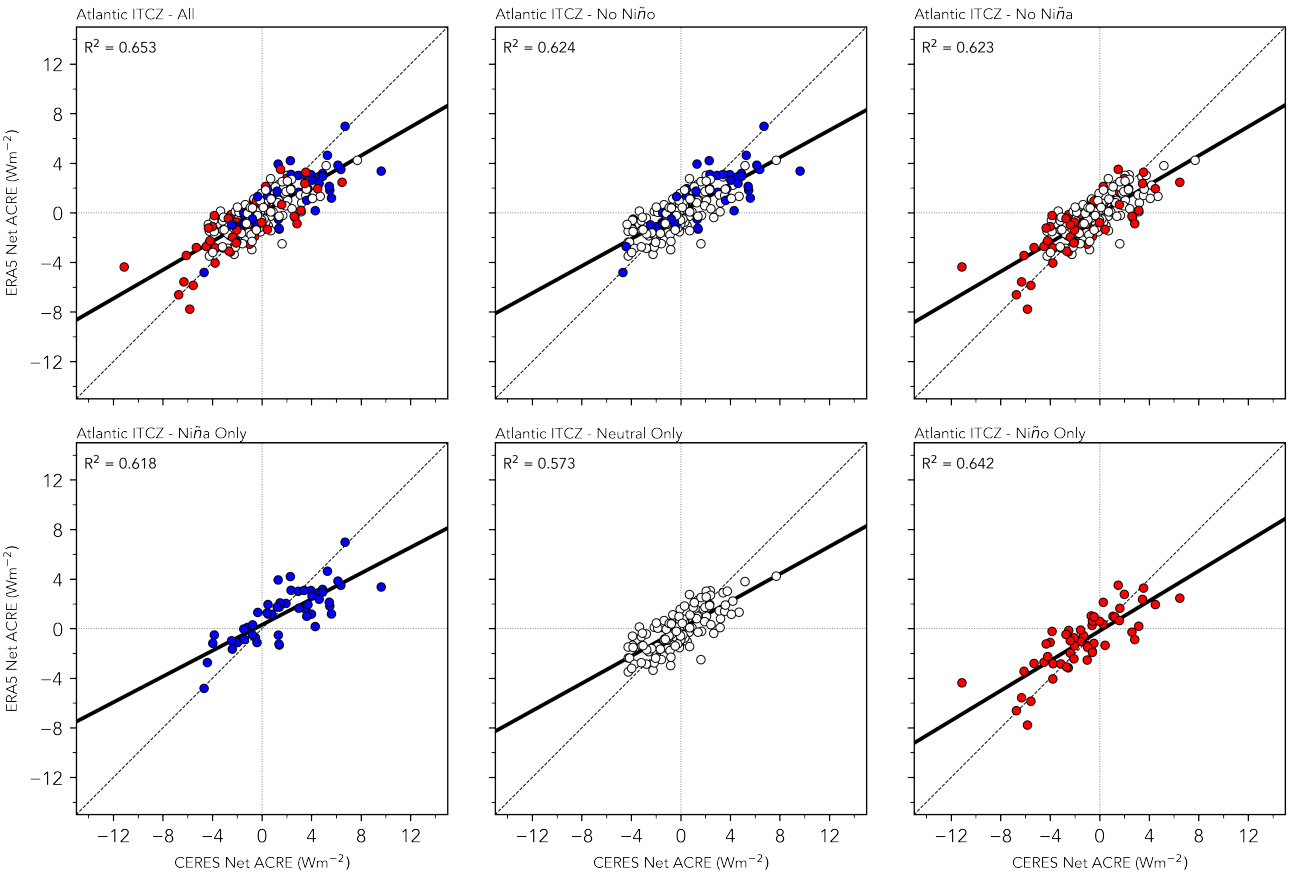

Figure S8. Same as Fig. S4, but for the SPCZ region

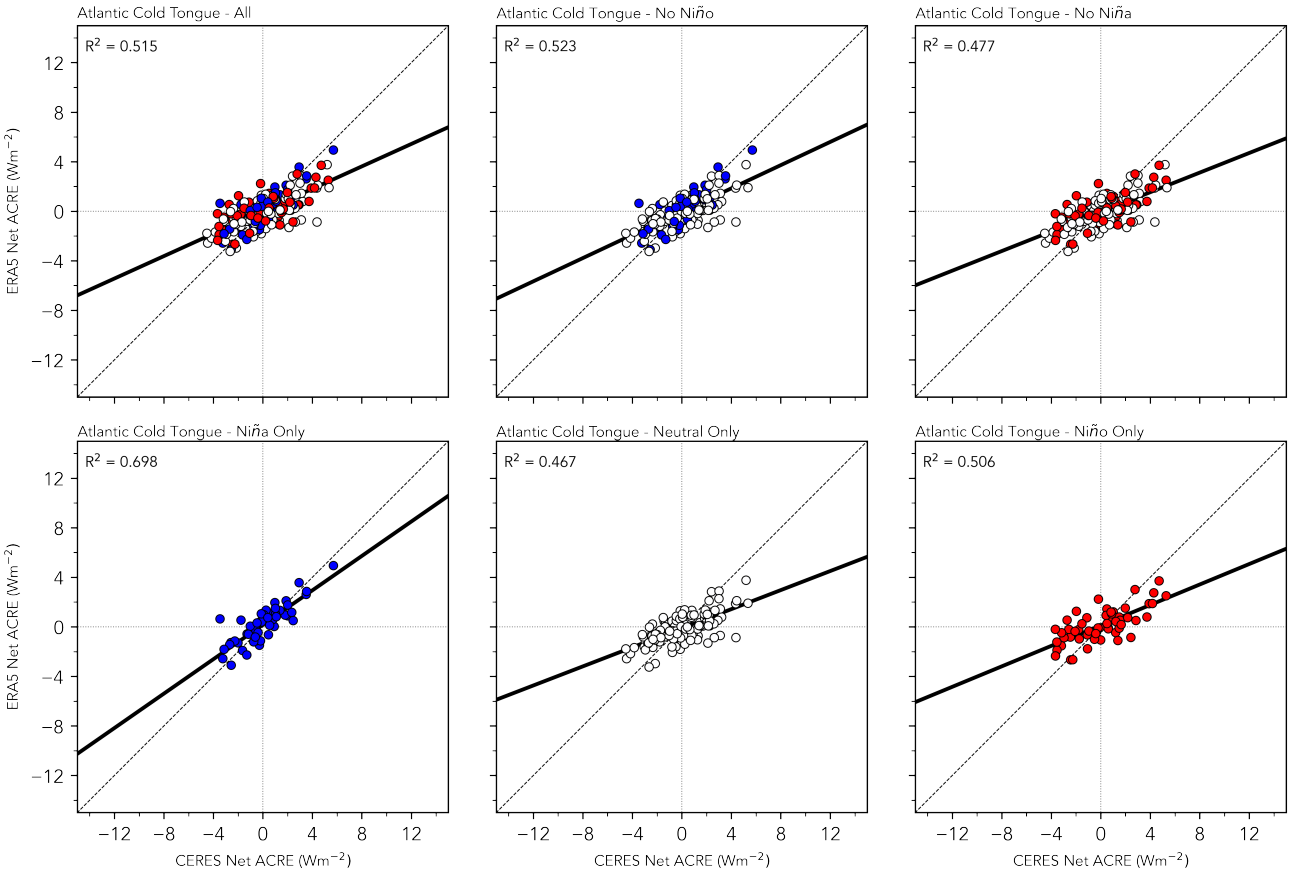

Figure S9. Same as Fig. S4, but for the Atlantic cold tongue region